

Urinary MicroRNA-Based Diagnostic Model for Central Nervous System Tumors Using Nanowire Scaffolds

Yotaro Kitano,[○] Kosuke Aoki,^{*○} Fumiharu Ohka, Shintaro Yamazaki, Kazuya Motomura, Kuniaki Tanahashi, Masaki Hirano, Tsuyoshi Naganawa, Mikiko Iida, Yukihiro Shiraki, Tomohide Nishikawa, Hiroyuki Shimizu, Junya Yamaguchi, Sachi Maeda, Hidenori Suzuki, Toshihiko Wakabayashi, Yoshinobu Baba, Takao Yasui,^{*} and Atsushi Natsume^{*}

Cite This: *ACS Appl. Mater. Interfaces* 2021, 13, 17316–17329

Read Online

ACCESS |

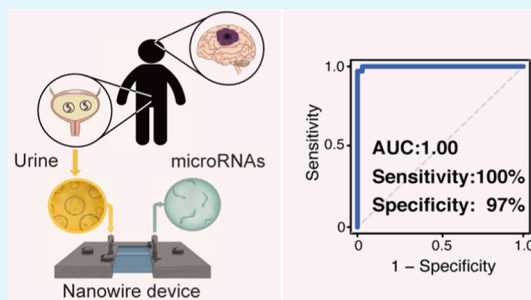
Metrics & More

Article Recommendations

Supporting Information

ABSTRACT: There are no accurate mass screening methods for early detection of central nervous system (CNS) tumors. Recently, liquid biopsy has received a lot of attention for less-invasive cancer screening. Unlike other cancers, CNS tumors require efforts to find biomarkers due to the blood–brain barrier, which restricts molecular exchange between the parenchyma and blood. Additionally, because a satisfactory way to collect urinary biomarkers is lacking, urine-based liquid biopsy has not been fully investigated despite the fact that it has some advantages compared to blood or cerebrospinal fluid-based biopsy. Here, we have developed a mass-producible and sterilizable nanowire-based device that can extract urinary microRNAs efficiently. Urinary microRNAs from patients with CNS tumors ($n = 119$) and noncancer individuals ($n = 100$) were analyzed using a microarray to yield comprehensive microRNA expression profiles. To clarify the origin of urinary microRNAs of patients with CNS tumors, glioblastoma organoids were generated. Glioblastoma organoid-derived differentially expressed microRNAs (DEMs) included 73.4% of the DEMs in urine of patients with parental tumors but included only 3.9% of those in urine of noncancer individuals, which suggested that many CNS tumor-derived microRNAs could be identified in urine directly. We constructed the diagnostic model based on the expression of the selected microRNAs and found that it was able to differentiate patients and noncancer individuals at a sensitivity and specificity of 100 and 97%, respectively, in an independent dataset. Our findings demonstrate that urinary microRNAs extracted with the nanowire device offer a well-fitted strategy for mass screening of CNS tumors.

KEYWORDS: urine-based liquid biopsy, microRNA, central nervous system tumor, organoid, nanowire



INTRODUCTION

Although cancer mortality over the past two decades has declined, mainly as a result of advances in early detection and treatment, the mortality rate specifically due to central nervous system (CNS) tumors has not declined.^{1,2} This is partly because hardly anyone will undergo regular medical checkups for CNS tumors until the tumors spread and neurological deficits are presented. Conventional brain medical checkups such as computed tomography (CT) and magnetic resonance imaging (MRI) are sensitive. However, these neuroradiological tests are time-consuming and costly, and are factors that prevent timely mass screening of CNS tumors. A sensitive, accurate, fast, and low-cost mass screening method for early detection of rare and lethal tumors like CNS tumors is strongly desired.³

Liquid biopsy using microRNAs (miRNAs) in biofluids (e.g., blood, cerebrospinal fluid, and urine) has received a lot of attention for early cancer detection and screening.⁴ miRNAs are small noncoding RNAs comprising 19–24 nucleotides

(nt), and miRNA expression profiles of cancer samples are different from those of noncancer samples.⁵ miRNAs are secreted from various cells and exist stably in biofluids within extracellular vesicles (EVs; these are sometimes referred to as exosomes).^{6,7} Several research groups have reported that miRNAs in blood could be used in clinical applications of cancer screening.^{8–10} Urine-based liquid biopsy has some advantages compared to blood-based liquid biopsy, such as being noninvasive and easy handling and sampling. Since urine sampling can be self-performed and repeated at any location and with a minimal effort,¹¹ urinary miRNAs seem to be the best biomarker candidate for cancer screening. However, urine-

Received: January 27, 2021

Accepted: March 15, 2021

Published: April 1, 2021



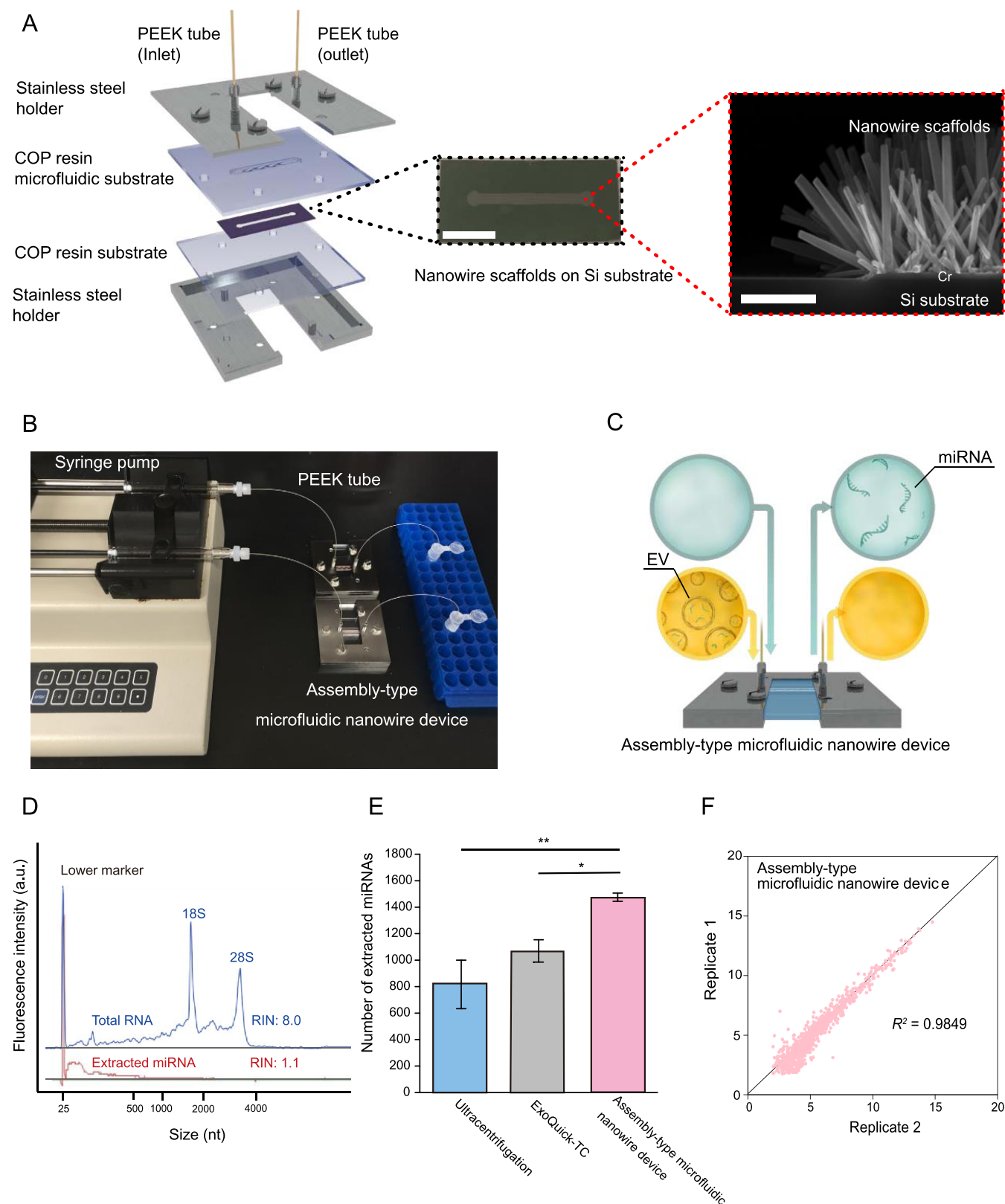


Figure 1. Assembly-type microfluidic nanowire device. (A) Schematic illustration of the assembly-type microfluidic nanowire device (left panel), photograph of the ZnO nanowire scaffolds on the Si substrate (middle panel; scale bar, 1 cm), and vertical cross-sectional field-emission scanning electron microscopic image of nanowire scaffolds grown on the Si substrate (right panel; scale bar, 1 μm). (B) Photograph of a system using the assembly-type microfluidic nanowire device. A 1 mL sample aliquot and lysis buffer were introduced into the nanowire device through a PEEK tube using a syringe pump. (C) Schematic illustration of a system to extract urinary miRNAs. First, urine was introduced into the nanowire device to capture EVs and EV-free miRNAs (yellow). Next, lysis buffer was introduced to extract EV-encapsulated miRNAs from the captured EVs by dissolving them and to collect EV-free miRNAs by releasing from the nanowires (green). (D) Electropherograms of the extracted miRNAs (red) and total RNA (blue). For the extracted miRNAs, a high peak was observed in the miRNA (25 nt) region but not in the 18S (1900 nt) or 28S

Figure 1. continued

(4700 nt) ribosomal RNA region, indicating high-purity miRNAs. (E) Bar graph illustrating the number of captured miRNAs in noncancer individuals as obtained by ultracentrifugation (cyan; $n = 3$), ExoQuick-TC (gray; $n = 3$), and the assembly-type microfluidic nanowire device (pink; $n = 100$). Data are represented as mean \pm standard error; * $P < 0.05$; ** $P < 0.01$ (Wilcoxon rank sum test). (F) Scatterplot of miRNA expression levels from the microarray data indicated reproducibility of technical replicates in the assembly-type microfluidic nanowire device. The coefficient of determination (R^2) was 0.9849.

based liquid biopsy has not been fully investigated for patients with nonurological tumors because none of the conventional methodologies (e.g., ultracentrifugation and polymeric precipitation methods like ExoQuick-TC) have a satisfactory way to collect urinary miRNAs.^{12,13} Although we previously developed a nanowire device for collection of urinary miRNAs, the device was not suitable for actual medical use because it was not sterilizable and could not be mass-produced.¹⁴

Identifying CNS tumors by miRNA-based liquid biopsy is highly challenging, due to the blood–brain barrier (BBB), which tightly regulates the movement between the blood and brain parenchyma.¹⁵ In addition, there are no studies that have adequately explained the origin of miRNAs in biofluids or that have explained their characteristic functions for patients with CNS tumors.

Here, first, we have developed a sterilizable and mass-producible zinc oxide (ZnO) nanowire-based device for extracting urinary miRNAs efficiently with a long-term goal of achieving liquid biopsy using urinary miRNAs. This nanowire device needs only 1 mL of urine and can extract a significantly greater variety and quantity of urinary miRNAs compared to ultracentrifugation and ExoQuick-TC. Next, we generated CNS tumor organoids to clarify the origin of urinary miRNA characteristics of patients with CNS tumors. Organoids have emerged as an alternative *in vitro* system to recapitulate tissues in a dish^{16,17} and secrete EV-encapsulated miRNAs and EV-free miRNAs as well as tumor cells.¹⁸ We extracted miRNAs of urine and culture supernatants of CNS tumor-derived organoids with our device and performed miRNA microarray analysis. We also performed enrichment analysis on target gene sets of tumor-derived urinary miRNAs to clarify their function. Finally, we extracted urinary miRNAs from urine samples from patients with CNS tumors and noncancer individuals. Microarray analysis of urinary miRNAs revealed a characteristic miRNA expression pattern, and based on it, we constructed a diagnostic model of patients with CNS tumors.

RESULTS

Assembly-Type Microfluidic Nanowire Device. We designed an assembly-type microfluidic nanowire device for extracting urinary miRNAs and acquiring miRNA expression profiles (Movie S1). We fabricated the assembly-type microfluidic nanowire device by two processes: first, we grew ZnO nanowire scaffolds from a thermally oxidized chromium layer on a silicon (Si) substrate; and second, we assembled the ZnO nanowire scaffolds, cyclo-olefin polymer (COP) resin microfluidic substrate, COP resin substrate, two stainless steel holders, and polyether ether ketone (PEEK) tubes into the device (Figure 1A). The device was connected to PEEK tubes for introduction of urine and lysis buffer and collection of flow-through urine and miRNA-containing solution (Figure 1B). Since no bonding process was required, each component of the assembly-type microfluidic nanowire device could be sterilized, such as by autoclave treatments, ethanol treatments, and dry-

heat treatments, to prevent contamination by miRNAs in saliva and sweat of persons handling the device. Furthermore, by simplifying the fabricating processes, fabrication time was shortened and the device could be mass-produced.

In situ extraction of urinary miRNAs within 40 min was demonstrated in two steps: first, a 1 mL urine sample was introduced into the device to capture EVs and EV-free miRNAs (20 min); and second, a 1 mL lysis buffer aliquot was introduced to extract EV-encapsulated miRNAs from the captured EVs by dissolving them and to collect EV-free miRNAs by releasing from the nanowires (20 min) (Figure 1C). The EVs and EV-free miRNAs are negatively charged. Since the ZnO nanowires have a positively charged surface, they can achieve highly efficient collection of EVs and EV-free miRNAs. Moreover, the large surface area of the nanowires and the microfluidic structure of the device contribute to the increase of capture efficiency.¹⁴

Performance of the Assembly-Type Microfluidic Nanowire Device. To investigate whether our assembly-type microfluidic nanowire device could extract urinary miRNAs efficiently, we extracted urinary miRNAs from noncancer individuals. The quality of miRNAs extracted from all samples was checked with an Agilent 2100 Bioanalyzer. Since a high peak was observed in the miRNA (25 nt) region but not in the 18S (1900 nt) or 28S (4700 nt) ribosomal RNA region (Figure 1D), the extracted urinary miRNAs were high-purity miRNAs. All urinary miRNAs were analyzed using a miRNA microarray and that yielded comprehensive miRNA expression profiles, which included 2565 species of miRNAs. Compared to the ultracentrifugation method ($n = 3$) or ExoQuick-TC ($n = 3$), the assembly-type nanowire device ($n = 100$) showed a significantly higher number of extracted miRNAs ($P = 0.01$ or 0.03 , respectively) and fluorescence intensity (both $P < 0.01$) in the miRNA microarray analysis of noncancer individuals (Figures 1E and S1A). We also compared the number of miRNAs identified in two or more cases between our nanowire device and the two conventional methods. Although miRNAs identified by ultracentrifugation ($n = 22/2388$ [0.92%]) and ExoQuick-TC ($n = 15/2381$ [0.63%]) accounted for less than 1% of the total, miRNAs identified by the nanowire device accounted for more than 50% (Figure S1B). Conclusively, the assembly-type nanowire device can extract a greater variety and quantity of urinary miRNAs than that by ultracentrifugation and ExoQuick-TC. The assembly-type nanowire device required less time and urine volume compared to the conventional methods in miRNA extraction (Table S1). In addition, to assess the reproducibility of the assembly-type nanowire device, we extracted miRNAs from duplicate urinary samples and performed microarray analyses, and showed that the nanowire device had high reproducibility of extracted miRNA species ($R^2 = 0.9849$) (Figure 1F). The assembly-type microfluidic nanowire device was found to be sterilizable, mass-producible, time-saving for miRNA extraction, and efficient and reproducible for miRNA extraction.

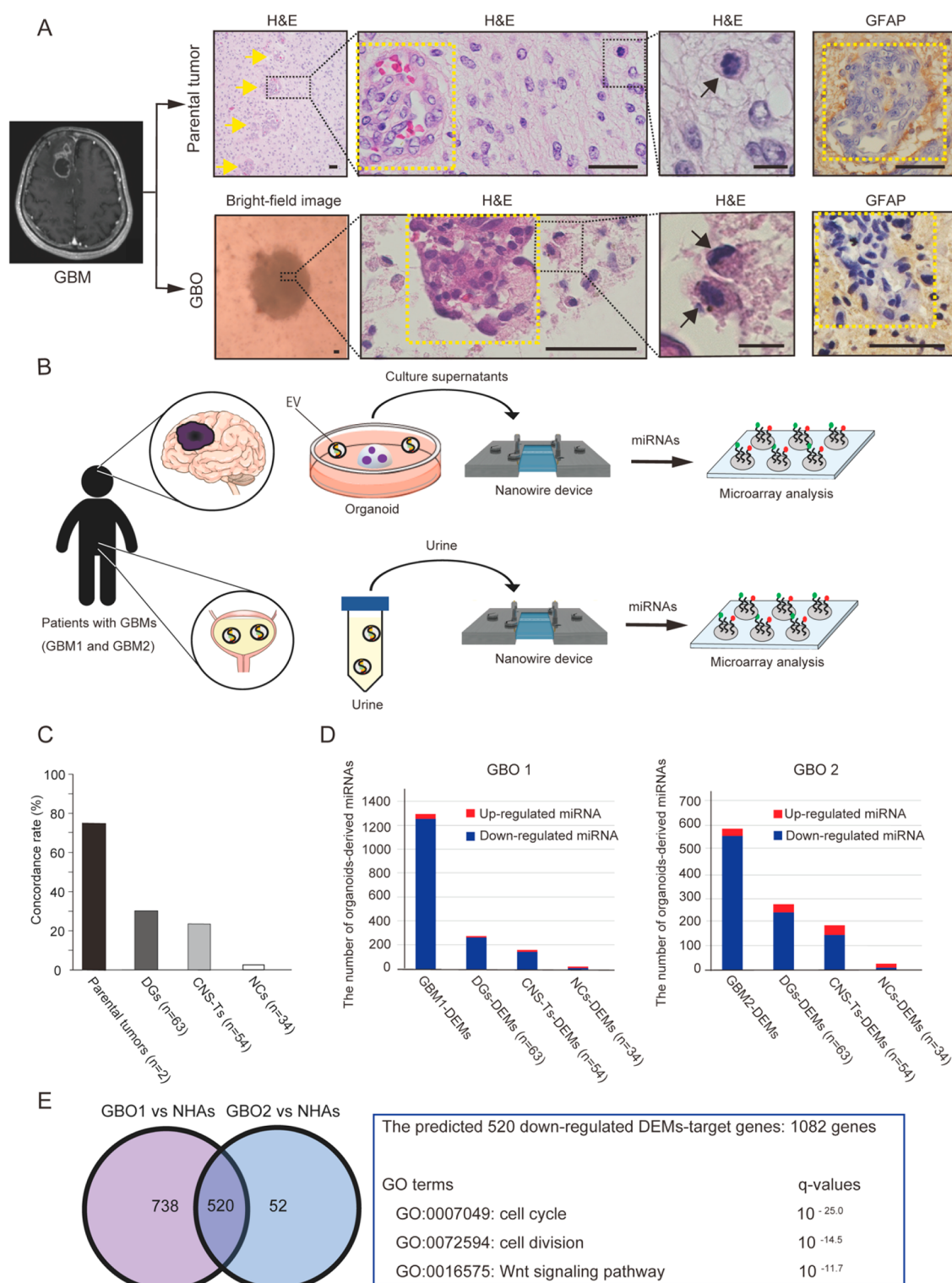


Figure 2. GBM organoid-derived miRNAs. (A) Parental tumor and corresponding GBM organoid (GBO). Parental tumor (upper row): sample H&E staining and immunostaining for glial fibrillary acidic protein (GFAP) images. GBO (lower row): sample bright-field image of GBO, sample H&E staining, and immunostaining for GFAP images of GBO. Scale bars, 50 μ m. Microvascular proliferation (yellow arrows and yellow dotted squares) and tumor cells (black arrows) were observed in both the parental tumor and GBO. (B) Schematic diagram of the analyses of miRNAs extracted from organoids and urine of the patients with parental tumors. (C) Percentages of organoid-derived DEMs in urinary DEMs of each group. Data are represented as mean. DGs, diffuse gliomas; CNS-Ts, central nervous system tumors (not including diffuse gliomas); and NCs, noncancer individuals. (D) Number of organoid-derived DEMs that indicate the same (up- or downregulated) tendency of the expression level of urinary DEMs in each group. (E) Venn diagram of overlapped downregulated miRNAs from two groups (left panel). Results of GO analysis suggested that the suppression of these miRNAs could activate several genes associated with tumorigenesis in GBM (right panel).

Table 1. Participants' Characteristics^a

characteristics	training set (<i>n</i> = 134)	validation set (<i>n</i> = 68)	<i>P</i>	exploratory set (<i>n</i> = 15)	organoid generation (<i>n</i> = 2)
Patients with CNS Tumor					
total	68	34		15	2
age, median (range), y	53 (21–86)	56 (14–81)	0.24	34 (2–63)	51 (44–58)
gender					
male	32 (47.1)	21 (61.8)	0.21	7 (46.7)	0
female	36 (52.9)	13 (38.2)		8 (53.3)	2 (100)
miRNA concentrations, average	0.40 ng/μL	0.58 ng/μL	0.27	0.75 ng/μL	0.23 ng/μL
histologic findings			0.67		
diffuse glioma	40 (58.8)	23 (67.7)			
glioblastoma	16	12		N/A	2 (100)
glioblastoma, IDH-mutant	4	3		N/A	1
glioblastoma, IDH-wild type	12	9		N/A	1
lower-grade glioma	24	11		N/A	N/A
diffuse astrocytoma, IDH-mutant	5	3		N/A	N/A
Diffuse astrocytoma, IDH-wild type	3	3		N/A	N/A
Anaplastic astrocytoma, IDH-mutant	2	1		N/A	N/A
Anaplastic astrocytoma, IDH-wild type	3	1		N/A	N/A
oligodendroglioma, IDH-mutant and 1p/19q-codeleted	9	3		N/A	N/A
anaplastic oligodendroglioma, IDH-mutant and 1p/19q-codeleted	2	0		N/A	N/A
meningioma	21 (30.9)	7 (20.6)		N/A	N/A
WHO grade I	20	6		N/A	N/A
grade II	0	1		N/A	N/A
grade III	1	0		N/A	N/A
Schwannoma	5 (7.4)	2 (5.9)		N/A	N/A
metastatic tumor	2 (2.9)	2 (5.9)		N/A	N/A
CNS neuroblastoma	N/A	N/A		3	N/A
pilocytic astrocytoma	N/A	N/A		2	N/A
CNS embryonal tumor, NOS	N/A	N/A		1	N/A
DNT	N/A	N/A		1	N/A
ependymoma	N/A	N/A		1	N/A
epidermoid cyst	N/A	N/A		1	N/A
gangliocytoma	N/A	N/A		1	N/A
ganglioglioma	N/A	N/A		1	N/A
MVNT	N/A	N/A		1	N/A
pituitary adenoma	N/A	N/A		1	N/A
primary CNS lymphoma	N/A	N/A		1	N/A
SFT/HPC	N/A	N/A		1	N/A
Noncancer Individuals					
total	66	34		N/A	N/A
age, median (range), y	41.5 (20–70)	40 (20–75)	0.81	N/A	N/A
gender					
male	36 (54.5)	22 (64.7)	0.4	N/A	N/A
female	30 (45.5)	12 (35.3)		N/A	N/A
miRNA concentrations, average	0.28 ng/μL	0.25 ng/μL	0.55	N/A	N/A

^aUnless otherwise specified, data are presented in number (percentage).

Origin of Urinary miRNA Characteristics of Patients with CNS Tumors. To assess whether the urinary miRNAs that showed significantly higher or lower expression in patients with CNS tumors were derived from the tumor itself, we established two glioblastoma (GBM) organoids (named GBOs) from patients with GBM (GBM1 and GBM2). Since organoids are *in vitro* three-dimensional (3D) cell aggregates derived from the primary tissue, the organoids have been reported to maintain the histological features, gene expression, and mutational profiles of their corresponding parental tumors,^{16,17} and organoid-secreted EV-encapsulated miRNAs

and EV-free miRNAs could be detected in organoid culture supernatants as well as tumor cells.¹⁸ Targeted-capture sequencing for GBOs and corresponding parental tumors demonstrated that most gene mutations were consistent between them, 95.1% in GBM1 and 100% in GBM2 (Figure S2). Actually, the GBOs showed similar histological features as well as mutational profiles to parental tumors (Figure 2A). Our nanowire device featured the capability of extracting miRNAs from cell culture supernatants (Figure S3). A 1 mL cell culture supernatant sample was introduced into the device to capture EVs and EV-free miRNAs, and then, a 1 mL lysis buffer aliquot

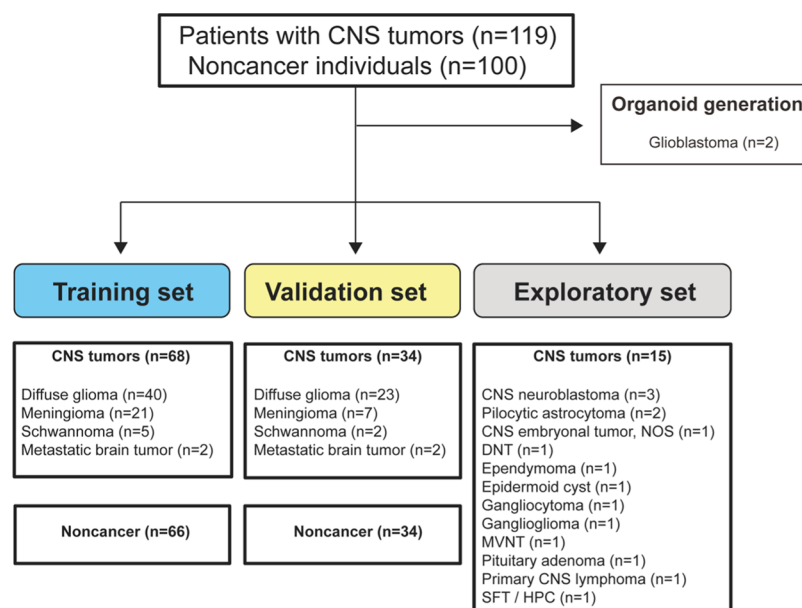


Figure 3. Workflow for developing the diagnostic model. Urine samples were obtained from 119 patients with CNS tumors and 100 noncancer individuals. The sample set was divided into three groups: the training set, validation set, and exploratory set.

was introduced to extract EV-encapsulated miRNAs from the captured EVs by dissolving them and to collect EV-free miRNAs by releasing from the nanowires. We extracted miRNAs from culture supernatants of two GBOs and immortalized human astrocytes (NHAs) ($n = 2$) with the nanowire device and performed miRNA microarray analyses. Differentially expressed miRNAs (DEMs) of GBO were defined as miRNAs that showed 1.5 times higher or lower expression (absolute fold-change >1.5) in culture supernatants of each GBO compared to the average expression in culture supernatants of NHAs.

We also extracted urinary miRNAs from two patients for whom organoids were established and 117 patients with CNS tumors, and performed miRNA microarray analyses (Figure 2B and Table 1). Urinary DEMs were defined in urine of patients with parental tumors, diffuse gliomas (GBMs and lower-grade gliomas (LGGs); $n = 63$), and other CNS tumors (not including diffuse gliomas; $n = 54$) and noncancer individuals who were randomly selected from 100 noncancer individuals ($n = 34$), as compared with the other noncancer individuals ($n = 66$) (absolute fold-change >1.5). On investigating whether DEMs of each GBO corresponded to urinary DEMs of patients with parental tumors, diffuse gliomas, and other CNS tumors and noncancer individuals, DEMs of the organoid culture supernatant were much more frequently identified as DEMs in urine of patients with parental tumors (73.4%), diffuse gliomas (30.6%), and other CNS tumors (25.0%) than the urine of noncancer individuals (3.9%) (Figure 2C). To delineate that organoid-derived miRNAs can be detected in blood as well as urine, we obtained serum miRNA data of patients with CNS tumors and noncancer individuals from the National Center for Biotechnology Information (NCBI) Gene Expression Omnibus (GEO) database. Serum DEMs were defined in serum of patients with diffuse gliomas ($n = 170$) and other CNS tumors (not including diffuse gliomas; $n = 89$) and noncancer individuals who were randomly selected from 157 noncancer individuals ($n = 52$), as compared with the other noncancer individuals ($n = 105$) (absolute fold-change >1.5).

DEMs of the organoid culture supernatant were much more frequently identified as DEMs in serum of patients with diffuse gliomas (62.2%) and other CNS tumors (60.9%) than serum of noncancer individuals (12.4%), the same as we found with urinary DEMs (Figure S4). These results suggested that many tumor-derived DEMs could be detected in urine as well as serum of patients with parental tumors directly.

The numbers of DEMs in both organoid culture supernatant and urine of each patient were 1299 and 603 (Figure 2D), respectively, and among them, 527 miRNAs (7 upregulated miRNAs and 520 downregulated miRNAs) were overlapped in both cases (Figures 2E and S5). Since it has been recognized that miRNAs regulate gene expression by binding some messenger RNAs (mRNAs),⁵ we searched in ENCORI (starBase v3.0), which is an open-source platform for studying miRNA–mRNA interactions, to identify the target genes of DEMs that overlapped in two GBOs. Using ENCORI, we were able to obtain biological targets of miRNAs by searching in seven databases (microT, miRanda, miRmap, PicTar, PITA, RNA22, and TargetScan). Four out of seven upregulated DEMs that overlapped in two GBOs were listed in ENCORI, while 117 out of 520 downregulated DEMs were listed as of November 15, 2020; however, the specific target genes of most miRNAs remain unknown. We performed Gene Ontology (GO) enrichment analysis using Metascape software to investigate the functions of upregulated and downregulated miRNAs in GBOs compared to NHAs (Figures 2E and S5). Targets of 117 downregulated miRNAs were significantly enriched in the pathways, which are known to be associated with tumorigenesis and activated in GBMs (i.e., cell cycle, cell division, and Wnt signaling pathway).^{19,20} It has been generally recognized that miRNAs negatively regulate gene expression at the post-transcriptional level.⁵ These results suggested that the suppression of tumor-derived miRNAs could activate several tumor-associated pathways, and these miRNAs could be detected in urine of patients with GBMs using our nanowire device.

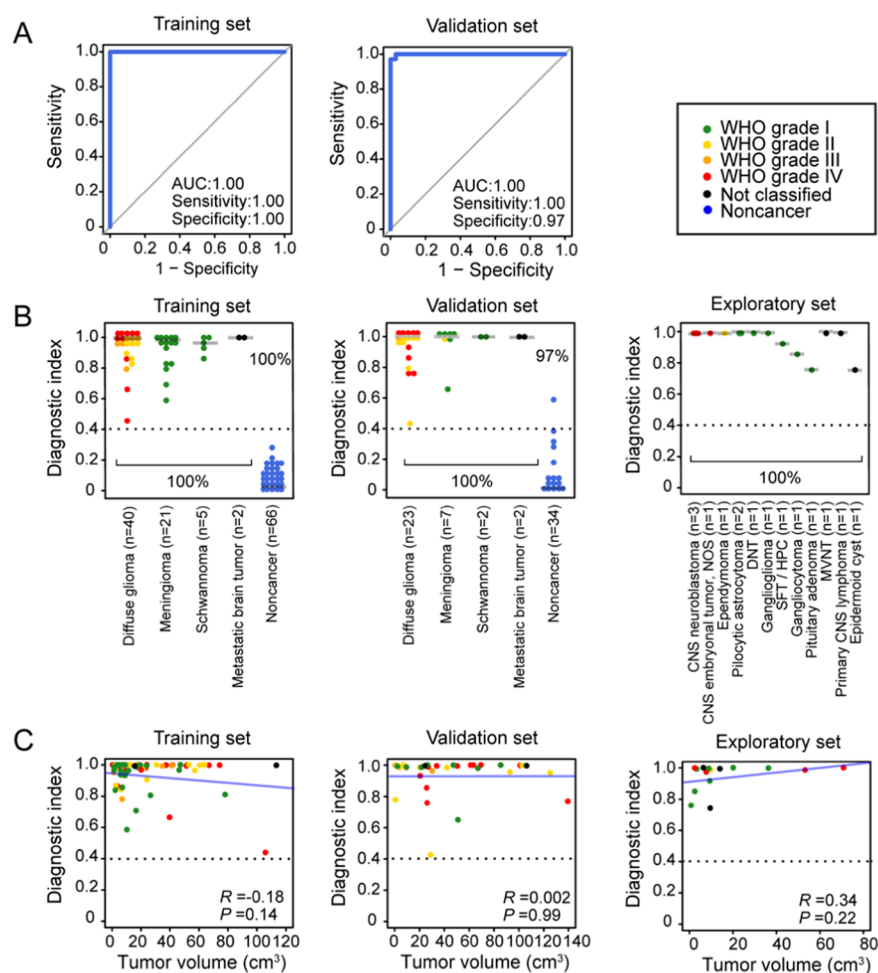


Figure 4. CNS tumor diagnostic model based on the 23-urinary miRNA classifier. Left panel, training set; middle panel, validation set; and right panel, exploratory set. (A) ROC curves for detecting patients with CNS tumors using 23 miRNAs selected for the diagnostic model. (B) Diagnostic index in each set. Each diagnostic accuracy (%) is indicated. The horizontal axis represents histological diagnosis of the CNS tumors. The gray lines represent the median value of each subgroup and the dotted lines represent the diagnostic index of 0.4. (C) Association between the tumor volume (cm^3) and diagnostic index. Pearson's correlation R and P values (Kruskal–Wallis rank sum test) are indicated. The blue lines represent the regression lines.

Identification of the Best Combination of miRNAs for Detection of CNS Tumors.

To evaluate the usefulness of the assembly-type microfluidic nanowire device for CNS tumor screening, we developed a diagnostic model for CNS tumors using the miRNA expression profiles. To construct a discriminant function as a diagnostic model between patients with CNS tumors and noncancer individuals, we randomly divided 100 noncancer individuals and 102 patients with CNS tumors (i.e., diffuse gliomas, meningiomas, schwannomas, and metastatic brain tumors) into two groups designated as the training set and the validation set (Figure 3). The training set had twice as many members as the validation set. No statistically significant differences were found in age, gender, miRNA concentration, and histologic findings between patients with CNS tumors and noncancer individuals in the training set or validation set (Table 1). The remaining CNS tumor patients ($n = 15$) were allocated to an exploratory set, which was intended to evaluate whether the model could also detect other kinds of CNS tumors: CNS neuroblastoma ($n = 3$), pilocytic astrocytoma ($n = 2$), CNS embryonal tumor, NOS ($n = 1$), dysembryoplastic neuroepithelial tumor (DNT) ($n = 1$), ependymoma ($n = 1$), epidermoid cyst ($n = 1$), gangliocytoma ($n = 1$), ganglioglioma ($n = 1$), multinodular

and vacuolating neuronal tumor of the cerebrum (MVNT) ($n = 1$), pituitary adenoma ($n = 1$), primary CNS lymphoma ($n = 1$), and solitary fibrous tumor/hemangiopericytoma (SFT/HPC) ($n = 1$). On the basis of the microarray results, we identified a total of 57 miRNAs that showed significantly higher or lower expression (absolute fold-change >1.5 and $P < 0.05$) in the patients with CNS tumors compared to noncancer individuals in the training set; 22 miRNAs were upregulated and 35 miRNAs were downregulated in patients with CNS tumors (Figure S6).

Next, logistic least absolute shrinkage and selection operator regression analysis (logistic LASSO regression analysis) was performed to select the most useful biomarkers among the 57 differentially expressed miRNAs (Figure S7); as a result, a 23-miRNA classifier was developed with data from the training set (miR-6070, miR-22-3p, miR-4538, miR-1285-3p, miR-372-5p, miR-4525, miR-5698, miR-204-3p, miR-6763-5p, miR-101-5p, miR-208a-5p, miR-371a-3p, miR-378a-5p, miR-216a-5p, miR-6864-3p, miR-450b-3p, miR-640, miR-4426, miR-17-3p, miR-450a-2-3p, miR-1248, miR-100-5p, and miR-16-5p). The diagnostic index was calculated based on the individualized values of 23 miRNAs to differentiate between patients with CNS tumors and noncancer individuals (Table S2):

Diagnostic index = $-0.2333 + \text{miR-6070} \times (0.3359) + \text{miR-22-3p} \times (0.3087) + \text{miR-4538} \times (0.1244) + \text{miR-1285-3p} \times (0.1097) + \text{miR-372-5p} \times (0.0246) + \text{miR-4525} \times (0.0194) + \text{miR-5698} \times (0.0059) + \text{miR-204-3p} \times (-0.0003) + \text{miR-6763-5p} \times (-0.0021) + \text{miR-101-5p} \times (-0.0106) + \text{miR-208a-5p} \times (-0.0142) + \text{miR-371a-3p} \times (-0.0591) + \text{miR-378a-5p} \times (-0.0873) + \text{miR-216a-5p} \times (-0.1004) + \text{miR-6864-3p} \times (-0.1024) + \text{miR-450b-3p} \times (-0.1565) + \text{miR-640} \times (-0.1607) + \text{miR-4426} \times (-0.3587) + \text{miR-17-3p} \times (-0.3744) + \text{miR-450a-2-3p} \times (-0.3744) + \text{miR-1248} \times (-0.3981) + \text{miR-100-5p} \times (-0.4780) + \text{miR-16-5p} \times (-0.5498)$.

Since the receiver operating characteristic (ROC) analysis is a tool used to describe the discrimination accuracy of a diagnostic model,²¹ we produced the ROC curve by plotting sensitivity (true-positive rate) on the y-axis against 1-specificity (false-positive rate) on the x-axis for the various diagnostic index values in the training set (Figure 4A). Each (x, y) coordinate on the plot represented the true-positive rate and the false-positive rate associated with a cutoff value for defining positive and negative. The cutoff value of the diagnostic model was determined to be 0.4 based on the Youden index²² (sensitivity + specificity - 1) in the training set (Figure 4B); a diagnostic index ≥ 0.4 indicated a CNS tumor, and a diagnostic index < 0.4 indicated its absence. The area under the ROC curve (AUC) was used to discriminate whether or not the CNS tumor was present, and we followed the established criteria that an AUC of 0.5 represents a test with no discriminating ability, while an AUC of 1.0 represents a test with perfect discrimination.²³ This diagnostic model provided the best discrimination in the training set; and the following values were obtained: AUC, 1.00 (95% confidence interval (CI), 1.00–1.00); sensitivity, 1.00; and specificity, 1.00 (Figure 4A,B). The performance of the diagnostic model was confirmed using the validation set, and the model was very accurate: AUC, 1.00 (95% CI, 1.00–1.00); sensitivity, 1.00; and specificity, 0.97 (Figure 4A).

Accuracy of the 23-miRNA-Based Diagnostic Model for CNS Tumor Screening. Our diagnostic model was found to be able to accurately discriminate CNS tumors from noncancer samples irrespective of the tumor grade (Figure 4B, left and middle panels); the World Health Organization's (WHO) classification of CNS tumors comprises a histological grading into four distinct grades of malignancy: WHO grades I–IV. In addition, the model also successfully classified all CNS tumors ($n = 15$) in the exploratory set as positive: sensitivity, 1.00 (Figure 4B, right panel). Next, we investigated whether our model could identify small CNS tumors. The diagnostic index of our model did not show a statistically significant association with tumor volume in the training set ($P = 0.14$), validation set ($P = 0.99$), and exploratory set ($P = 0.22$) (Figure 4C). In particular, CNS tumors with a volume of 1 cm³ or less were observed in 2, 3, and 1 cases in the training set, validation set, and exploratory set, respectively. Even in these cases, the diagnostic index was extremely high: median (range), 0.98 (0.76–1.00). Accordingly, our diagnostic model was found to be able to accurately discriminate CNS tumors from noncancer samples irrespective of the tumor grade and size. Thus, we judged this combination of 23 miRNAs as a promising biomarker for CNS tumor screening.

DISCUSSION

There is a growing interest in precision oncology for liquid biopsies because they are noninvasive and suitable for massive diagnosis screening. Indeed, many attempts are now being made to extract biomarker candidates and use them for early cancer detection.^{24,25} For example, Si nanowire devices have been developed, which directly identify tumor antigens by attaching antitumor marker antibodies on the surface, e.g., antiprostata-specific antigen antibody for prostate cancers.²⁶ However, sensitive tumor-specific markers for CNS tumors have not been identified in biofluids partially due to the BBB. Since EVs can easily pass through the BBB via transcytosis,²⁷ we focused on an efficient way to capture EVs in urine. To the best of our knowledge, we have developed the first device that achieved high collection efficiency of urinary miRNAs (i.e., EV-encapsulated miRNAs and EV-free miRNAs) from patients with CNS tumors; realization of such devices has been believed to be a challenge for collecting miRNAs through the BBB. Assembly of the devices, their integration into systems, and usability aspects are crucial to transferring the devices from the laboratory to the scientific community, and they are key for clinical studies. Reproducible quality of the devices and reproducibility of tumor detections are prerequisites to translational research to humans.

CNS tumors, especially in diffuse gliomas, inevitably transform into more aggressive tumors and they recur in many cases.²⁸ Gross total resection is significantly correlated with better prognosis,^{29,30} indicating that early detection of the tumor has great clinical significance. CNS tumors rarely induce subjective symptoms when relatively small, thus most patients will not undergo CT or MRI for tumor screening until the tumors have sufficiently spread. Our diagnostic model could accurately detect CNS tumors irrespective of the tumor grade and size, which demonstrates that it is an ideal screening method for CNS tumors. Since we have not examined cases with neurotrauma, neurological infections, or cancers other than CNS, either, further studies are strongly warranted.

Several previous reports revealed that blood-based miRNA signatures could be useful for distinguishing patients with CNS tumors from noncancer individuals.^{31,32} However, none of those studies have completely explained the origin and function of those miRNAs and the percentage of miRNAs in the bloodstream that are derived from tumors themselves. Then, we generated CNS tumor organoids and investigated the origin and percentage of tumor-derived miRNAs in biofluids. Traditional patient-derived cell culture models (e.g., patient-derived cells and patient-derived xenografts) require serial passages to propagate tumor cells, which are not favorable to maintain various cellular subtypes and key driver gene expression of parental tumors.³³ In contrast, several groups have reported that organoids recapitulate inter- and intratumoral heterogeneity and maintain many key features of parental tumors; and GBOs also maintain histological and genetic mutational features of parental tumors.^{16,17} In this study, we also generated GBOs by modifying the previously reported method.¹⁶

Urinary DEMs of patients with parental tumors contained approximately 75% of the GBO-derived DEMs. GO analysis demonstrated that the target genes of DEMs in both GBO and urine were related to tumor genesis and progression. Given that many DEMs of GBO culture supernatants could be captured in the urine as DEMs, there is a possibility that the

urinary miRNA expression reflects slight changes in the tumor itself such as malignant transformation. At the same time, these results suggested that they reflect not only the expression of the miRNAs by the CNS tumors themselves but also by miRNAs whose expression levels are reactively changed by surrounding cells, including cells involved in inflammation, edema, and tumor immunity. Although anti-PD-1 antibodies have antitumor effects on many tumors, it is often difficult to determine the actual tumors in which they will be effective before use. For example, it has been reported that neoadjuvant therapy of anti-PD-1 antibody could be effective in patients with GBM, but an easy way is needed to determine in which specific patients it will be effective before resorting to surgery.^{34,35} If the urinary miRNA expression pattern related to the efficacy of the anti-PD-1 antibody can be clarified, it will play a role in treatment decision for patients with CNS tumors. The fact that the number of GBOs that we created and analyzed is only two is a limitation of the study. Further investigations are needed.

In this study, the nanowire device enabled us to extract a larger quantity of urinary miRNAs than conventional methods, analyze them comprehensively using the microarray, and develop the accurate diagnostic model for CNS tumors. In the future, examining only 23 miRNAs selected for the diagnostic model in this study will allow diagnosis of CNS tumors by nonexpensive methods such as real-time reverse transcription polymerase chain reaction (PCR). Furthermore, the methodology of our study can be applied to different types of cancer, which benefits the development of diagnostic models for pancreatic cancer using only 1 mL of urine.

CONCLUSIONS

In summary, we developed a sterilizable and mass-producible ZnO nanowire-based device that could extract a significantly greater variety and quantity of miRNAs from urine. Analysis of the organoid-derived miRNAs revealed that the miRNA expression pattern of the tumors themselves greatly affected the urinary miRNA expression. The diagnostic model based on the urinary miRNA expression could distinguish patients with CNS tumors from noncancer individuals accurately. These results point to the suitability of urinary miRNA profiles for noninvasive CNS tumor mass screening and in the future will be a useful means to identify phenotypic changes in CNS tumors such as malignant transformation.

MATERIALS AND METHODS

Fabrication Procedure for ZnO Nanowires on a Si Substrate. A Si substrate (Advantech Co., Ltd.) was cleaned, a positive photoresist (OFPR8600, Tokyo Ohka Kogyo Co., Ltd.) was coated onto it, and then the channel pattern was formed by photolithography. Next, a 140 nm thick chromium (Cr) layer was deposited on the patterned substrate using an electron cyclotron resonance sputtering device (Elionix Inc.). After removal of the photoresist, the Cr layer was thermally oxidized at 400 °C for 2 h; the thermally oxidized Cr layer was a seed layer for the ZnO nanowire growth. The ZnO nanowires were grown by immersing the substrate in a solution mixture of 15 mM hexamethylenetetramine (FUJIFILM Wako Corp.) and 15 mM zinc nitrate hexahydrate (Thermo Fisher Scientific Inc.) at 95 °C for 3 h. The nanowires grown on the substrate were cleaned using Millipore water and allowed to air-dry overnight in a vacuum desiccator.

Clinical Samples. A total of 119 urine and tumor samples were obtained from patients with CNS tumors, admitted in 14 hospitals in Japan (Table S3) between March 2017 and July 2020. All urine

samples were obtained before surgery. We also obtained 100 urine samples from noncancer individuals. All urine samples were centrifuged (15 min, 4 °C, 3000g) to remove cellular debris and apoptotic bodies³⁶ and stored at −80 °C until used. Tumor samples were obtained intraoperatively. DNA was extracted from tumors using the QIAamp DNA Mini Kit (Qiagen N.V.) according to the manufacturer's instructions. The amount of DNA obtained was quantified using the Qubit dsDNA HS Assay Kit (Thermo Fisher Scientific Inc.). Mutations in *IDH1* and *IDH2* were analyzed using Sanger sequencing or droplet digital PCR as previously described.³⁷ Chromosomal codeletion of 1p and 19q was analyzed using SALSA MLPA Kits P088 (MRC Holland b.v.) according to the manufacturer's instructions. CNS tumors were classified according to the 2016 revision of the WHO Classification of Tumors of the Central Nervous System.³⁸ Board-certified neurosurgeons measured tumor volumes on gadolinium-enhanced T1-weighted or fluid-attenuated inversion recovery MRI sequencing images. Tumor volumes were calculated as follows: Tumor volume (cm³) = major axis (cm) × minor axis (cm) × height (cm) × $\pi/6$. A written informed consent was obtained from all participants. This study was approved by the ethics committees or institutional review boards of all participating institutes.

Generation of Glioblastoma Organoids (GBOs). Fresh surgically resected glioblastoma tissues were put into sterile phosphate-buffered saline (PBS; Thermo Fisher Scientific Inc.). These tissues were immediately minced into 1 mm² pieces using sterilized surgical scalpel blades (Futaba Co., Ltd.) in Gibco Neurobasal Medium (Thermo Fisher Scientific Inc.) supplemented with N2 Supplement, B27 Supplement, minus vitamin A, Recombinant Human FGF basic, EGF Human Recombinant Protein, heparin sodium, and L-glutamine (but not fetal bovine serum (FBS)). To remove red blood cells and debris, the pieces were incubated in 5 mL of organoid culture medium, Gibco Neurobasal Medium, containing 15 μ L of ACK lysing buffer (Thermo Fisher Scientific Inc.) and 5 μ L of Collagenase, Type IV (Thermo Fisher Scientific Inc.) at room temperature, and then mechanically dissociated by pipetting. Dissociated cells were collected by centrifuging (500g for 3 min at 4 °C) and resuspended in Matrigel Basement Membrane Matrix (Corning Inc.), which was diluted with the same amount of the organoid culture medium. Then, 350 μ L of the suspended matrigel mixture was seeded in each well of a 6-well plate, incubated for 30 min at 37 °C and 5% CO₂ to solidify it, and finally overlaid with 2 mL of the organoid culture medium. Live organoid images were obtained with a BZ-X710 microscope (KEYENCE Corp.).

H&E Staining and Immunohistochemistry (IHC). Parental tumor and organoid tissues were fixed in 10% neutral-buffered formalin, dehydrated, and embedded in paraffin; 5 μ m thick sections were put onto slides in preparation for H&E staining (which was performed using conventional methods) and IHC. After deparaffinization and hydration, the slides were incubated in a retrieval solution (10 mM, pH 6.0) for 20 min at 100 °C in an electric pod. Endogenous peroxidase was inhibited using 3% H₂O₂ with methanol for 5 min at room temperature. The slides were subsequently blocked in a Dako Antibody Diluent (Agilent Technologies Inc.) for 10 min at room temperature. Mouse monoclonal anti-GFAP antibody (Abcam plc) was used as a primary antibody, which was diluted with blocking buffer, and applied to the slides and incubated for 2 h at room temperature. Goat anti-mouse IgG H&L (HRP polymer; Abcam plc) for anti-GFAP antibody was applied as a secondary antibody and incubated for 1 h at room temperature. Then, the 3,3'-diaminobenzidine (DAB) peroxidase [horseradish peroxidase (HRP)] Substrate Kit (Vector Laboratories, Inc.) was used according to the manufacturer's instructions for the visualization of the bound primary antibody. Slides were counterstained with Mayer's hematoxylin solution (Sakura Finetek Japan Co., Ltd.).

Targeted-Capture Sequencing. DNA was extracted from formalin-fixed and paraffin-embedded organoids and parental tumors using the QIAamp DNA FFPE Tissue Kit (QIAGEN N.V.) and blood samples using the QIAamp DNA Mini Kit (QIAGEN N.V.) following the manufacturer's instructions. The amount of DNA obtained was

quantified using the Qubit dsDNA HS Assay Kit (Thermo Fisher Scientific Inc.). Sequencing libraries were prepared according to the manufacturers' protocols using the KAPA Hyper Prep Kit (Roche Ltd.), SureSelect XT target enrichment system, and ClearSeq SS Comprehensive Cancer bait that targeted 151 cancer-associated genes (Agilent Technologies Inc.). Prepared libraries were run on a Miseq next-generation sequencing platform with 2×75 -bp end reads (Illumina Inc.) for paired samples. The obtained reads were aligned to the hg19 reference genome using the Burrows Wheeler aligner with default parameters and a -mem option.³⁹ Polymerase chain reaction duplicates were removed using Picard tools (<http://broadinstitute.github.io/picard/>). Sequence variations were detected and annotated using Mutect2,⁴⁰ and we adopted the variants that fulfilled the following criteria: (i) number of variant reads ≥ 10 ; (ii) number of reads ≥ 30 ; and (iii) variant allele frequency (VAF) ≥ 0.05 . We excluded the following: (i) number of variant reads in normal sample > 2 and (ii) VAF in normal sample ≥ 0.02 . We annotated the adopted variants with ANNOVAR (<http://annovar.openbioinformatics.org/en/latest/>) and excluded the variants that met at least one of the following criteria: (i) synonymous and ambiguously annotated (unknown) variants and (ii) common single nucleotide polymorphisms, which were defined as those with $\geq 1\%$ allele frequency in the Exome Aggregation Consortium (<http://exac.broadinstitute.org/>), the 1000 Genomes Project (<http://www.internationalgenome.org/>), and the National Heart, Lung, and Blood Institute Exome Sequencing Project 6500 (<https://evs.gs.washington.edu/EVS/>).

Culture Supernatants of Patient-Derived GBOs. miRNAs derived from GBOs were collected from culture supernatants in one well of a six-well plate.^{9,41} After changing to fresh medium (not including FBS), GBOs were incubated for 48 h. The culture supernatant was collected and centrifuged at 2000g for 10 min at 4 °C. To thoroughly remove cellular debris, the supernatant was filtered through a 0.22 μm filter (Merck Millipore Corp.). The supernatant was stored at -80°C until used.

Culture Supernatants of Normal Human Astrocytes (NHAs). NHAs were kindly provided by Dr. R. Pieper (University of California, San Francisco, San Francisco, CA).^{42,43} This cell line was authenticated in the original cell bank and was tested to be mycoplasma-free when resuscitated. NHA cells were cultured with Dulbecco's modified Eagle's medium-high glucose (DMEM; Sigma-Aldrich Corp.) containing 10% FBS and 1% penicillin/streptomycin (Thermo Fisher Scientific Inc.). NHA cells were maintained at 37 °C in a humidified incubator with 5% CO_2 . EVs derived from cells were collected from culture supernatants in one well of a six-well plate.^{9,41} The cells were washed with PBS, and the culture medium was replaced with advanced DMEM (not including FBS). After incubation for 48 h, the culture supernatant was collected and centrifuged at 2000g for 10 min at 4 °C. To thoroughly remove cellular debris, the supernatant was filtered through a 0.22 μm filter (Merck Millipore Corp.). The supernatant was stored at -80°C until used.

Extracting miRNAs in Urine and Derived from GBOs and NHAs Using the Nanowire Device. We fabricated the nanowire device by assembling ZnO nanowire scaffolds, COP resin microfluidic substrate, COP resin substrate, two stainless steel holders, and PEEK tubes (Figure 1A). After assembling the device, the inlet PEEK tube was connected to a syringe pump (KDS-200, KD Scientific Inc.) to introduce urine or culture supernatant and lysis buffer. On the other hand, the outlet PEEK tube was put in an RNase-free microfuge tube (Eppendorf AG.) to collect the flow-through urine or culture supernatant and miRNA-containing solution (Figure 1B). Extracting miRNAs by the assembly-type microfluidic nanowire device consisted of two steps: capturing of EVs and EV-free miRNAs on nanowires, and *in situ* extraction of miRNAs from EVs and release of EV-free miRNAs from nanowires. First, a 1 mL sample aliquot (urine or cell culture supernatants) was introduced into the assembly-type microfluidic nanowire device at a flow rate of 50 $\mu\text{L}/\text{min}$ using a syringe pump (Figure 1C). The miRNA extraction from the captured EVs and EV-free miRNAs released from the nanowires was performed using cell lysis buffer M (20 mM tris-HCl (pH 7.4), 200 mM sodium chloride, 2.5 mM magnesium chloride, and 0.05 w/v% NP-40

substitute; FUJIFILM Wako Corp.), which was introduced at a flow rate of 50 $\mu\text{L}/\text{min}$ using the syringe pump. The assembly-type microfluidic nanowire device could capture EVs and EV-free miRNAs from 1 mL sample aliquots, and extract EV-encapsulated miRNAs from the captured EVs by dissolving them and collecting EV-free miRNAs by releasing from the nanowires using the lysis buffer within 40 min (capture, 20 min; extraction, 20 min) (Movie S1). The quality of miRNAs extracted from all samples was checked with an Agilent 2100 Bioanalyzer (Agilent Technologies Inc.) (Figures 1D and S3). We used microarray-based urinary miRNA expression data, which had been obtained by ultracentrifugation, with ExoQuick-TC in our previous study¹⁴ to compare the performance of miRNA extraction with the performance of the assembly-type microfluidic nanowire device (Table S1).

Microarray Analysis of miRNA Expression. The miRNA solution extracted with lysis buffer was purified using the SeraMir Exosome RNA Purification Kit (System Biosciences Inc.) according to the manufacturer's instructions. miRNA concentrations were measured on the Qubit 3.0 fluorometer (Thermo Fisher Scientific Inc.), using the Qubit microRNA Assay Kit (Thermo Fisher Scientific Inc.). Then, 15 μL of purified miRNA was analyzed for the miRNA profile using the 3D-Gene Human miRNA Oligo chip ver.21 (Toray Industries Inc.). 3D-Gene was designed to use fluorescent signals to detect 2565 miRNA sequences registered in miRBase release 21 (<http://www.mirbase.org/>). From the output signal data, we subtracted the background noise and calibrated the remainder using the global normalization method⁴⁴ with the median value as 25.

Public Database Analyses. Accession code GSE139031 data were downloaded from the NCBI GEO database (<https://www.ncbi.nlm.nih.gov/geo/>). These serum miRNA microarray (3D-Gene Human miRNA Oligo chip ver.21)-based data were obtained from 259 patients with CNS tumors and 157 noncancer individuals. Downloaded raw data were normalized using the global normalization method as well as our data.

Developing the Diagnostic Model. Before performing statistical comparisons, patients with CNS tumors and noncancer individuals were assigned to three sets: patients with diffuse gliomas, meningiomas, schwannomas, or metastatic brain tumors ($n = 102$) and noncancer individuals were randomly divided into the training set and validation set and patients with the remaining types of CNS tumors ($n = 15$) were assigned to the exploratory set (Figure 3). The training set had twice as many members as the validation set, and it was used to select miRNAs and develop the diagnostic model. The validation set was used to validate the diagnostic performance of the model.

According to a combination of some miRNAs, we developed the diagnostic model in which the signal intensity values of miRNAs were used as explanatory variables. The combination of miRNAs was selected in two steps. First, in the training set, comparisons between two groups (patients with CNS tumors vs noncancer individuals) were made to detect differentially expressed miRNAs using the Wilcoxon rank sum test. An absolute fold-change greater than 1.5 (calculated with each miRNA signal intensity value plus 0.1) and a $P < 0.05$ were used as the cutoff criteria. Next, the candidate miRNAs were selected from differentially expressed miRNAs using logistic LASSO regression analysis with 10-fold cross validation.⁴⁵ The diagnostic performance was evaluated by calculating the area under the ROC curve values, sensitivity, and specificity. The Youden index (sensitivity + specificity - 1) was used to determine the cutoff value of the diagnostic model.²²

Prediction and Enrichment Analysis of Target Genes of Selected miRNAs *In Silico*. We used ENCORI (starBase v3.0; <http://starbase.sysu.edu.cn/index.php>) to identify the target genes of selected miRNAs.^{46,47} We narrowed the target genes under the strictest criteria in ENCORI as of November 15, 2020. Next, we used Metascape software (<http://metascape.org>) to perform GO analysis on the target genes as previously described.⁴⁸

Statistical Analyses. Statistical analyses were performed using Software R version 3.6.1 (<https://www.r-project.org/>). Differences in characteristics between the two groups were evaluated using the

Wilcoxon rank sum test (continuous variables) and Fisher's exact test (categorical variables). The Wilcoxon rank sum test was also used to compare the diagnostic values between the two groups using the "coin" package version 1.3-1. The Wilcoxon signed rank test was used to compare the fluorescence intensity of extracted miRNAs in each method using the coin package version 1.3-1. Logistic LASSO regression analysis was used to identify the candidate miRNAs for the diagnostic model with nonzero coefficients using the "glmnet" package version 3.0. Differences in diagnostic values among patients with different histopathological diagnoses and WHO grades were analyzed using the Kruskal–Wallis rank sum test. Associations of diagnostic values and tumor volumes were analyzed using the Pearson correlation analysis. The ROC curve analysis was performed, and diagnostic sensitivity, specificity, and AUC were calculated using the "pROC" package version 1.15.0. The q -values (false discovery rates) were adjusted using the Benjamini and Hochberg method.⁴⁹ P and q -values <0.05 were taken to indicate statistical significance.

Data and Material Availability. The microarray data that support this study are available through the NCBI database under the accession code GSE145510. All other data are available within the article and the [Supporting Information](#).

■ ASSOCIATED CONTENT

SI Supporting Information

The Supporting Information is available free of charge at <https://pubs.acs.org/doi/10.1021/acsami.1c01754>.

Capability for urinary miRNA extraction in each method (Figure S1); GBM organoids maintain mutational profiles of corresponding parental tumors (Figure S2); quality of the extracted miRNAs obtained from cell culture supernatants (Figure S3); comparison of GBM organoid-derived miRNAs to serum miRNAs (Figure S4); GO analysis of overlapped upregulated miRNAs (Figure S5); volcano plot showing the differential expression of urinary miRNAs between patients with CNS tumors and noncancer individuals in the training set (Figure S6); construction of the 23-urinary miRNA classifier (Figure S7); comparison among methodologies (Table S1); constant term, explanatory variables, and partial regression coefficients in the diagnostic model (Table S2); and numbers of tumor samples obtained at 14 hospitals (Table S3) (PDF)

Concentrations of the extracted miRNAs (Data S1) (XLSX)

System of the assembly-type microfluidic nanowire device (Movie S1) (MP4)

■ AUTHOR INFORMATION

Corresponding Authors

Kosuke Aoki – Department of Neurosurgery, Graduate School of Medicine, Nagoya University, Showa-ku, Nagoya 466-8550, Japan; Institute of Nano-Life-Systems, Institutes of Innovation for Future Society, Nagoya University, Chikusa-ku, Nagoya 464-8603, Japan; orcid.org/0000-0002-3274-5272; Email: kaoki@med.nagoya-u.ac.jp; Fax: (+81) 52-744-2360

Takao Yasui – Institute of Nano-Life-Systems, Institutes of Innovation for Future Society and Department of Biomolecular Engineering, Graduate School of Engineering, Nagoya University, Chikusa-ku, Nagoya 464-8603, Japan; Japan Science and Technology Agency (JST), PRESTO, Kawaguchi, Saitama 332-0012, Japan; orcid.org/0000-0003-0333-3559; Email: yasui@chembio.nagoya-u.ac.jp; Fax: (+81) 52-789-4666

Atsushi Natsume – Department of Neurosurgery, Graduate School of Medicine, Nagoya University, Showa-ku, Nagoya 466-8550, Japan; Institute of Nano-Life-Systems, Institutes of Innovation for Future Society, Nagoya University, Chikusa-ku, Nagoya 464-8603, Japan; Email: anatsume@med.nagoya-u.ac.jp; Fax: (+81) 52-744-2360

Authors

Yotaro Kitano – Department of Neurosurgery, Graduate School of Medicine, Nagoya University, Showa-ku, Nagoya 466-8550, Japan; Department of Neurosurgery, Graduate School of Medicine, Mie University, Tsu 514-8507, Japan

Fumiharu Ohka – Department of Neurosurgery, Graduate School of Medicine, Nagoya University, Showa-ku, Nagoya 466-8550, Japan

Shintaro Yamazaki – Department of Neurosurgery, Graduate School of Medicine, Nagoya University, Showa-ku, Nagoya 466-8550, Japan

Kazuya Motomura – Department of Neurosurgery, Graduate School of Medicine, Nagoya University, Showa-ku, Nagoya 466-8550, Japan

Kuniaki Tanahashi – Department of Neurosurgery, Graduate School of Medicine, Nagoya University, Showa-ku, Nagoya 466-8550, Japan

Masaki Hirano – Department of Neurosurgery, Graduate School of Medicine, Nagoya University, Showa-ku, Nagoya 466-8550, Japan

Tsuyoshi Naganawa – Department of Biomolecular Engineering, Graduate School of Engineering, Nagoya University, Chikusa-ku, Nagoya 464-8603, Japan

Mikiko Iida – Department of Biomolecular Engineering, Graduate School of Engineering, Nagoya University, Chikusa-ku, Nagoya 464-8603, Japan

Yukihiro Shiraki – Department of Pathology, Graduate School of Medicine, Nagoya University, Showa-ku, Nagoya 466-8550, Japan

Tomohide Nishikawa – Department of Neurosurgery, Graduate School of Medicine, Nagoya University, Showa-ku, Nagoya 466-8550, Japan

Hiroyuki Shimizu – Department of Neurosurgery, Graduate School of Medicine, Nagoya University, Showa-ku, Nagoya 466-8550, Japan

Junya Yamaguchi – Department of Neurosurgery, Graduate School of Medicine, Nagoya University, Showa-ku, Nagoya 466-8550, Japan

Sachi Maeda – Department of Neurosurgery, Graduate School of Medicine, Nagoya University, Showa-ku, Nagoya 466-8550, Japan

Hidenori Suzuki – Department of Neurosurgery, Graduate School of Medicine, Mie University, Tsu 514-8507, Japan

Toshihiko Wakabayashi – Department of Neurosurgery, Graduate School of Medicine, Nagoya University, Showa-ku, Nagoya 466-8550, Japan

Yoshinobu Baba – Institute of Nano-Life-Systems, Institutes of Innovation for Future Society and Department of Biomolecular Engineering, Graduate School of Engineering, Nagoya University, Chikusa-ku, Nagoya 464-8603, Japan; Institute of Quantum Life Science, National Institutes for Quantum and Radiological Science and Technology, Inage-ku, Chiba 263-8555, Japan

Complete contact information is available at: <https://pubs.acs.org/doi/10.1021/acsami.1c01754>

Author Contributions

[○]Y.K. and K.A. contributed equally to this work.

Author Contributions

Y.K., K.A., H.S., T.W., Y.B., T.Y., and A.N. designed the study. Y.K., K.A., F.O., S.Y., K.M., K.T., M.H., Y.S., T.N., H.S., J.Y., S.M., and A.N. collected clinical specimens. Y.K., T.N., M.I., and T.Y. fabricated the experimental setups and performed microRNA extraction. F.O., S.Y., and M.H. generated glioblastoma organoids. Y.K. and K.A. performed all computational analyses. Y.K., K.A., Y.S., T.Y., and A.N. interpreted the results. Y.K., K.A., T.Y., and A.N. wrote the manuscript.

Notes

The authors declare no competing financial interest.

ACKNOWLEDGMENTS

This work was supported by a Grant-in-Aid for Scientific Research on Innovative Areas “Chemistry for Multimolecular Crowding Biosystems” (JSPS KAKENHI Grant no. 17H06356 to A.N.), a PRESTO (JST Grant no. JPMJPR19H9 to T.Y.), a Medical Research and Development Program (AMED Grand no. JP21he2302007 to T.Y. and A.N.), a SICORP (JST Grant no. JPMJSC19E3 to T.Y.), a Grant-in-Aid for Young Scientists (A) (JSPS KAKENHI Grant no. 17H04803 to T.Y.), a Grant-in-Aid for Scientific Research (S) (JSPS KAKENHI Grant no. 18H05243 to T.Y.), a Grant-in-Aid for Exploratory Research (JSPS KAKENHI Grant no. 20K21124 to T.Y.), and a Grant-in-Aid for Young Scientists (B) (JSPS KAKENHI Grant no. 17K16643 to K.A.).

ABBREVIATIONS

AUC, area under the curve
 BBB, blood–brain barrier
 CI, confidence interval
 CNS, central nervous system
 COP, cyclo-olefin polymer
 CT, computed tomography
 DEM, differentially expressed microRNA
 DNT, dysembryoplastic neuroepithelial tumor
 EV, extracellular vesicle
 FBS, fetal bovine serum
 GBM, glioblastoma
 GBO, glioblastoma organoid
 GEO, Gene Expression Omnibus
 GO, Gene Ontology
 IDH, isocitrate dehydrogenase
 IHC, immunohistochemistry
 LASSO, least absolute shrinkage and selection operator
 LGG, lower grade glioma
 mRNA, messenger RNAs
 miRNA, microRNA
 MRI, magnetic resonance imaging
 MVNT, multinodular and vacuolating neuronal tumor of the cerebrum
 N/A, not applicable
 NCBI, National Center for Biotechnology Information
 NHA, normal human astrocyte
 NOS, not otherwise specified
 nt, nucleotide
 PBS, phosphate-buffered saline
 PCR, polymerase chain reaction
 PDMS, poly(dimethylsiloxane)
 PEEK, polyether ether ketone

RIN, RNA integrity number

ROC, receiver operating characteristic

SFT/HPC, solitary fibrous tumor/hemangiopericytoma

Si, silicon

VAF, variant allele frequency

WHO, World Health Organization

ZnO, zinc oxide

REFERENCES

- (1) Siegel, R. L.; Miller, K. D.; Jemal, A. Cancer statistics, 2020. *Ca-Cancer J. Clin.* **2020**, *70*, 7–30.
- (2) Ostrom, Q. T.; Patil, N.; Cioffi, G.; Waite, K.; Kruchko, C.; Barnholtz-Sloan, J. S. CBTRUS Statistical Report: Primary Brain and Other Central Nervous System Tumors Diagnosed in the United States in 2013–2017. *Neuro-Oncology* **2020**, *22*, iv1–iv96.
- (3) Best, M. G.; Sol, N.; Zijl, S.; Reijneveld, J. C.; Wesseling, P.; Wurdinger, T. Liquid biopsies in patients with diffuse glioma. *Acta Neuropathol.* **2015**, *129*, 849–865.
- (4) Heitzer, E.; Perakis, S.; Geigl, J. B.; Speicher, M. R. The potential of liquid biopsies for the early detection of cancer. *npj Precis. Oncol.* **2017**, *1*, No. 36.
- (5) Bartel, D. P. MicroRNAs—Genomics, Biogenesis, Mechanism, and Function. *Cell* **2004**, *116*, 281–297.
- (6) Valadi, H.; Ekstrom, K.; Bossios, A.; Sjostrand, M.; Lee, J. J.; Lotvall, J. O. Exosome-mediated transfer of mRNAs and microRNAs is a novel mechanism of genetic exchange between cells. *Nat. Cell Biol.* **2007**, *9*, 654–659.
- (7) Pegtel, D. M.; Cosmopoulos, K.; Thorley-Lawson, D. A.; van Eijndhoven, M. A.; Hopmans, E. S.; Lindenberg, J. L.; de Gruij, T. D.; Wurdinger, T.; Middeldorp, J. M. Functional delivery of viral miRNAs via exosomes. *Proc. Natl. Acad. Sci. U.S.A.* **2010**, *107*, 6328–6333.
- (8) Shimomura, A.; Shiino, S.; Kawauchi, J.; Takizawa, S.; Sakamoto, H.; Matsuzaki, J.; Ono, M.; Takeshita, F.; Niida, S.; Shimizu, C.; Fujiwara, Y.; Kinoshita, T.; Tamura, K.; Ochiya, T. Novel combination of serum microRNA for detecting breast cancer in the early stage. *Cancer Sci.* **2016**, *107*, 326–334.
- (9) Yokoi, A.; Matsuzaki, J.; Yamamoto, Y.; Yoneoka, Y.; Takahashi, K.; Shimizu, H.; Uehara, T.; Ishikawa, M.; Ikeda, S. I.; Sonoda, T.; Kawauchi, J.; Takizawa, S.; Aoki, Y.; Niida, S.; Sakamoto, H.; Kato, K.; Kato, T.; Ochiya, T. Integrated extracellular microRNA profiling for ovarian cancer screening. *Nat. Commun.* **2018**, *9*, No. 4319.
- (10) Usuba, W.; Urabe, F.; Yamamoto, Y.; Matsuzaki, J.; Sasaki, H.; Ichikawa, M.; Takizawa, S.; Aoki, Y.; Niida, S.; Kato, K.; Egawa, S.; Chikaraishi, T.; Fujimoto, H.; Ochiya, T. Circulating miRNA panels for specific and early detection in bladder cancer. *Cancer Sci.* **2019**, *110*, 408–419.
- (11) Kim, H.; Park, S.; Jeong, I. G.; Song, S. H.; Jeong, Y.; Kim, C. S.; Lee, K. H. Noninvasive Precision Screening of Prostate Cancer by Urinary Multimarker Sensor and Artificial Intelligence Analysis. *ACS Nano* **2021**, *15*, 4054–4065.
- (12) Cheng, L.; Sun, X.; Scicluna, B. J.; Coleman, B. M.; Hill, A. F. Characterization and deep sequencing analysis of exosomal and non-exosomal miRNA in human urine. *Kidney Int.* **2014**, *86*, 433–444.
- (13) Sun, J.; Han, S.; Ma, L.; Zhang, H.; Zhan, Z.; Aguilar, H. A.; Zhang, H.; Xiao, K.; Gu, Y.; Gu, Z.; Tao, W. A. Synergistically Bifunctional Paramagnetic Separation Enables Efficient Isolation of Urine Extracellular Vesicles and Downstream Phosphoproteomic Analysis. *ACS Appl. Mater. Interfaces* **2021**, *13*, 3622–3630.
- (14) Yasui, T.; Yanagida, T.; Ito, S.; Konakade, Y.; Takeshita, T.; Naganawa, T.; Nagashima, K.; Shimada, T.; Kaji, N.; Nakamura, Y.; Thiodorus, A. I.; He, Y.; Rahong, S.; Kanai, M.; Yukawa, H.; Ochiya, T.; Kawai, T.; Baba, Y. Unveiling massive numbers of cancer-related urinary-microRNA candidates via nanowires. *Sci. Adv.* **2017**, *3*, No. e1701133.
- (15) Abbott, N. J.; Patabendige, A. A.; Dolman, D. E.; Yusof, S. R.; Begley, D. J. Structure and function of the blood-brain barrier. *Neurobiol. Dis.* **2010**, *37*, 13–25.

- (16) Jacob, F.; Salinas, R. D.; Zhang, D. Y.; Nguyen, P. T. T.; Schnoll, J. G.; Wong, S. Z. H.; Thokala, R.; Sheikh, S.; Saxena, D.; Prokop, S.; Liu, D. A.; Qian, X.; Petrov, D.; Lucas, T.; Chen, H. L.; Dorsey, J. F.; Christian, K. M.; Binder, Z. A.; Nasrallah, M.; Brem, S.; O'Rourke, D. M.; Ming, G. L.; Song, H. A Patient-Derived Glioblastoma Organoid Model and Biobank Recapitulates Inter- and Intra-tumoral Heterogeneity. *Cell* **2020**, *180*, 188–204.
- (17) Golebiewska, A.; Hau, A. C.; Oudin, A.; Stieber, D.; Yabo, Y. A.; Baus, V.; Barthelemy, V.; Klein, E.; Bougnaud, S.; Keunen, O.; Wantz, M.; Michelucci, A.; Neirinckx, V.; Muller, A.; Kaoma, T.; Nazarov, P. V.; Azuaje, F.; De Falco, A.; Flies, B.; Richart, L.; Poovathingal, S.; Arns, T.; Grzyb, K.; Mock, A.; Herold-Mende, C.; Steino, A.; Brown, D.; May, P.; Miletic, H.; Malta, T. M.; Noushmehr, H.; Kwon, Y. J.; Jahn, W.; Klink, B.; Tanner, G.; Stead, L. F.; Mittelbronn, M.; Skupin, A.; Hertel, F.; Bjerkvig, R.; Niclou, S. P. Patient-derived organoids and orthotopic xenografts of primary and recurrent gliomas represent relevant patient avatars for precision oncology. *Acta Neuropathol.* **2020**, *140*, 919–949.
- (18) Szvicsek, Z.; Oszvald, A.; Szabo, L.; Sandor, G. O.; Kelemen, A.; Soos, A. A.; Paloczi, K.; Harsanyi, L.; Tolgyes, T.; Dede, K.; Bursics, A.; Buzas, E. I.; Zeold, A.; Wiener, Z. Extracellular vesicle release from intestinal organoids is modulated by *Apc* mutation and other colorectal cancer progression factors. *Cell. Mol. Life Sci.* **2019**, *76*, 2463–2476.
- (19) Shinohara, H.; Yagita, H.; Ikawa, Y.; Oyaizu, N. Fas Drives Cell Cycle Progression in Glioma Cells Via Extracellular Signal-Regulated Kinase Activation. *Cancer Res.* **2000**, *60*, 1766–1772.
- (20) Pulvirenti, T.; Van Der Heijden, M.; Droms, L. A.; Huse, J. T.; Tabar, V.; Hall, A. Dishevelled 2 signaling promotes self-renewal and tumorigenicity in human gliomas. *Cancer Res.* **2011**, *71*, 7280–7290.
- (21) Obuchowski, N. A.; Bullen, J. A. Receiver operating characteristic (ROC) curves: review of methods with applications in diagnostic medicine. *Phys. Med. Biol.* **2018**, *63*, No. 07TR01.
- (22) Fluss, R.; Faraggi, D.; Reiser, B. Estimation of the Youden Index and its associated cutoff point. *Biom. J.* **2005**, *47*, 458–472.
- (23) Hoo, Z. H.; Candlish, J.; Teare, D. What is an ROC curve? *Emerg. Med. J.* **2017**, *34*, 357–359.
- (24) Song, P.; Ye, D.; Zuo, X.; Li, J.; Wang, J.; Liu, H.; Hwang, M. T.; Chao, J.; Su, S.; Wang, L.; Shi, J.; Wang, L.; Huang, W.; Lal, R.; Fan, C. DNA Hydrogel with Aptamer-Toehold-Based Recognition, Cloaking, and Decloaking of Circulating Tumor Cells for Live Cell Analysis. *Nano Lett.* **2017**, *17*, 5193–5198.
- (25) Dong, S.; Wang, Y.; Liu, Z.; Zhang, W.; Yi, K.; Zhang, X.; Zhang, X.; Jiang, C.; Yang, S.; Wang, F.; Xiao, X. Beehive-Inspired Macroporous SERS Probe for Cancer Detection through Capturing and Analyzing Exosomes in Plasma. *ACS Appl. Mater. Interfaces* **2020**, *12*, 5136–5146.
- (26) Smith, R.; Duan, W.; Quarterman, J.; Morris, A.; Collie, C.; Black, M.; Toor, F.; Salem, A. K. Surface Modifying Doped Silicon Nanowire Based Solar Cells for Applications in Biosensing. *Adv. Mater. Technol.* **2019**, *4*, No. 1800349.
- (27) Morad, G.; Carman, C. V.; Hagedorn, E. J.; Perlin, J. R.; Zon, L. I.; Mustafaoğlu, N.; Park, T. E.; Ingber, D. E.; Daisy, C. C.; Moses, M. A. Tumor-Derived Extracellular Vesicles Breach the Intact Blood-Brain Barrier via Transcytosis. *ACS Nano* **2019**, *13*, 13853–13865.
- (28) Suzuki, H.; Aoki, K.; Chiba, K.; Sato, Y.; Shiozawa, Y.; Shiraiishi, Y.; Shimamura, T.; Niida, A.; Motomura, K.; Ohka, F.; Yamamoto, T.; Tanahashi, K.; Ranjit, M.; Wakabayashi, T.; Yoshizato, T.; Kataoka, K.; Yoshida, K.; Nagata, Y.; Sato-Otsubo, A.; Tanaka, H.; Sanada, M.; Kondo, Y.; Nakamura, H.; Mizoguchi, M.; Abe, T.; Muragaki, Y.; Watanabe, R.; Ito, I.; Miyano, S.; Natsume, A.; Ogawa, S. Mutational landscape and clonal architecture in grade II and III gliomas. *Nat. Genet.* **2015**, *47*, 458–468.
- (29) Aoki, K.; Nakamura, H.; Suzuki, H.; Matsuo, K.; Kataoka, K.; Shimamura, T.; Motomura, K.; Ohka, F.; Shiina, S.; Yamamoto, T.; Nagata, Y.; Yoshizato, T.; Mizoguchi, M.; Abe, T.; Momii, Y.; Muragaki, Y.; Watanabe, R.; Ito, I.; Sanada, M.; Yajima, H.; Morita, N.; Takeuchi, I.; Miyano, S.; Wakabayashi, T.; Ogawa, S.; Natsume, A. Prognostic relevance of genetic alterations in diffuse lower-grade gliomas. *Neuro-Oncology* **2018**, *20*, 66–77.
- (30) Ellingson, B. M.; Abrey, L. E.; Nelson, S. J.; Kaufmann, T. J.; Garcia, J.; Chinot, O.; Saran, F.; Nishikawa, R.; Henriksson, R.; Mason, W. P.; Wick, W.; Butowski, N.; Ligon, K. L.; Gerstner, E. R.; Colman, H.; de Groot, J.; Chang, S.; Mellinghoff, I.; Young, R. J.; Alexander, B. M.; Colen, R.; Taylor, J. W.; Arrillaga-Romany, I.; Mehta, A.; Huang, R. Y.; Pope, W. B.; Reardon, D.; Batchelor, T.; Prados, M.; Galanis, E.; Wen, P. Y.; Cloughesy, T. F. Validation of postoperative residual contrast-enhancing tumor volume as an independent prognostic factor for overall survival in newly diagnosed glioblastoma. *Neuro-Oncology* **2018**, *20*, 1240–1250.
- (31) Zachariah, M. A.; Oliveira-Costa, J. P.; Carter, B. S.; Stott, S. L.; Nahed, B. V. Blood-based biomarkers for the diagnosis and monitoring of gliomas. *Neuro-Oncology* **2018**, *20*, 1155–1161.
- (32) Ohno, M.; Matsuzaki, J.; Kawachi, J.; Aoki, Y.; Miura, J.; Takizawa, S.; Kato, K.; Sakamoto, H.; Matsushita, Y.; Takahashi, M.; Miyakita, Y.; Ichimura, K.; Narita, Y.; Ochiya, T. Assessment of the Diagnostic Utility of Serum MicroRNA Classification in Patients With Diffuse Glioma. *JAMA Netw. Open* **2019**, *2*, No. e1916953.
- (33) Ledur, P. F.; Onzi, G. R.; Zong, H.; Lenz, G. Culture Conditions Defining Glioblastoma Cells Behavior: What Is the Impact for Novel Discoveries? *Oncotarget* **2017**, *8*, 69185–69197.
- (34) Schalper, K. A.; Rodriguez-Ruiz, M. E.; Diez-Valle, R.; Lopez-Janeiro, A.; Porciuncula, A.; Idoate, M. A.; Inoges, S.; de Andrea, C.; Lopez-Diaz de Cerio, A.; Tejada, S.; Berraondo, P.; Villarreal-Espindola, F.; Choi, J.; Gurrpide, A.; Giraldez, M.; Goicoechea, I.; Gallego Perez-Larraya, J.; Sanmamed, M. F.; Perez-Gracia, J. L.; Melero, I. Neoadjuvant nivolumab modifies the tumor immune microenvironment in resectable glioblastoma. *Nat. Med.* **2019**, *25*, 470–476.
- (35) Cloughesy, T. F.; Mochizuki, A. Y.; Orpilla, J. R.; Hugo, W.; Lee, A. H.; Davidson, T. B.; Wang, A. C.; Ellingson, B. M.; Rytlewski, J. A.; Sanders, C. M.; Kawaguchi, E. S.; Du, L.; Li, G.; Yong, W. H.; Gaffey, S. C.; Cohen, A. L.; Mellinghoff, I. K.; Lee, E. Q.; Reardon, D. A.; O'Brien, B. J.; Butowski, N. A.; Nghiemphu, P. L.; Clarke, J. L.; Arrillaga-Romany, I. C.; Colman, H.; Kaley, T. J.; de Groot, J. F.; Liao, L. M.; Wen, P. Y.; Prins, R. M. Neoadjuvant anti-PD-1 immunotherapy promotes a survival benefit with intratumoral and systemic immune responses in recurrent glioblastoma. *Nat. Med.* **2019**, *25*, 477–486.
- (36) Jeppesen, D. K.; Hvam, M. L.; Primdahl-Bengtson, B.; Boysen, A. T.; Whitehead, B.; Dyrskjot, L.; Orntoft, T. F.; Howard, K. A.; Ostfeld, M. S. Comparative analysis of discrete exosome fractions obtained by differential centrifugation. *J. Extracell. Vesicles* **2014**, *3*, No. 25011.
- (37) Hirano, M.; Ohka, F.; Maeda, S.; Chalise, L.; Yamamichi, A.; Aoki, K.; Kato, A.; Tanahashi, K.; Motomura, K.; Nishimura, Y.; Hara, M.; Shinjo, K.; Kondo, Y.; Wakabayashi, T.; Natsume, A. A novel high-sensitivity assay to detect a small fraction of mutant IDH1 using droplet digital PCR. *Brain Tumor Pathol.* **2018**, *35*, 97–105.
- (38) Louis, D. N.; Perry, A.; Reifenberger, G.; von Deisinger, A.; Figarella-Branger, D.; Cavenee, W. K.; Ohgaki, H.; Wiestler, O. D.; Kleihues, P.; Ellison, D. W. The 2016 World Health Organization Classification of Tumors of the Central Nervous System: a summary. *Acta Neuropathol.* **2016**, *131*, 803–820.
- (39) Li, H.; Durbin, R. Fast and accurate short read alignment with Burrows-Wheeler transform. *Bioinformatics* **2009**, *25*, 1754–1760.
- (40) Cibulskis, K.; Lawrence, M. S.; Carter, S. L.; Sivachenko, A.; Jaffe, D.; Sougnez, C.; Gabriel, S.; Meyerson, M.; Lander, E. S.; Getz, G. Sensitive detection of somatic point mutations in impure and heterogeneous cancer samples. *Nat. Biotechnol.* **2013**, *31*, 213–219.
- (41) Yokoi, A.; Yoshioka, Y.; Hirakawa, A.; Yamamoto, Y.; Ishikawa, M.; Ikeda, S.; Kato, T.; Niimi, K.; Kajiyama, H.; Kikkawa, F.; Ochiya, T. A Combination of Circulating Mirnas for the Early Detection of Ovarian Cancer. *Oncotarget* **2017**, *8*, 89811–89823.
- (42) Sonoda, Y.; Ozawa, T.; Hirose, Y.; Aldape, D. K.; McMahon, M.; Berger, S. M.; Pieper, O. R. Formation of Intracranial Tumors by Genetically Modified Human Astrocytes Defines Four Pathways

Critical in the Development of Human Anaplastic Astrocytoma. *Cancer Res.* **2001**, *61*, 4956–4960.

(43) Ohka, F.; Shinjo, K.; Deguchi, S.; Matsui, Y.; Okuno, Y.; Katsushima, K.; Suzuki, M.; Kato, A.; Ogiso, N.; Yamamichi, A.; Aoki, K.; Suzuki, H.; Sato, S.; Arul Rayan, N.; Prabhakar, S.; Goke, J.; Shimamura, T.; Maruyama, R.; Takahashi, S.; Suzumura, A.; Kimura, H.; Wakabayashi, T.; Zong, H.; Natsume, A.; Kondo, Y. Pathogenic Epigenetic Consequences of Genetic Alterations in IDH-Wild-Type Diffuse Astrocytic Gliomas. *Cancer Res.* **2019**, *79*, 4814–4827.

(44) Takahashi, I.; Hama, Y.; Matsushima, M.; Hirotsu, M.; Kano, T.; Hohzen, H.; Yabe, I.; Utsumi, J.; Sasaki, H. Identification of plasma microRNAs as a biomarker of sporadic Amyotrophic Lateral Sclerosis. *Mol. Brain* **2015**, *8*, No. 67.

(45) Duan, J.; Soussen, C.; Brie, D.; Idier, J.; Wan, M.; Wang, Y. P. Generalized LASSO with under-determined regularization matrices. *Signal Process.* **2016**, *127*, 239–246.

(46) Li, J. H.; Liu, S.; Zhou, H.; Qu, L. H.; Yang, J. H. starBase v2.0: decoding miRNA-ceRNA, miRNA-ncRNA and protein-RNA interaction networks from large-scale CLIP-Seq data. *Nucleic Acids Res.* **2014**, *42*, D92–D97.

(47) Deguchi, S.; Katsushima, K.; Hatanaka, A.; Shinjo, K.; Ohka, F.; Wakabayashi, T.; Zong, H.; Natsume, A.; Kondo, Y. Oncogenic effects of evolutionarily conserved noncoding RNA ECONEXIN on gliomagenesis. *Oncogene* **2017**, *36*, 4629–4640.

(48) Ranjit, M.; Hirano, M.; Aoki, K.; Okuno, Y.; Ohka, F.; Yamamichi, A.; Kato, A.; Maeda, S.; Motomura, K.; Matsuo, K.; Enomoto, A.; Ino, Y.; Todo, T.; Takahashi, M.; Wakabayashi, T.; Kato, T.; Natsume, A. Aberrant Active cis-Regulatory Elements Associated with Downregulation of RET Finger Protein Overcome Chemoresistance in Glioblastoma. *Cell Rep.* **2019**, *26*, 2274–2281.

(49) Benjamini, Y.; Hochberg, Y. Controlling the False Discovery Rate: A Practical and Powerful Approach to Multiple Testing. *J. R. Stat. Soc.* **1995**, *57*, 289–300.